^{27}Al($n,x\gamma$) reactions for neutron energies from 3 to 400 MeV

A. Pavlik, H. Hitzenberger-Schauer, and H. Vonach
Institut für Radiumforschung und Kernphysik, Universität Wien, A-1090 Wien, Austria

M. B. Chadwick, R. C. Haight, R. O. Nelson, and P. G. Young
Los Alamos National Laboratory, Los Alamos, New Mexico 87545
(Received 17 September 1997)

The prompt γ radiation from the interaction of fast neutrons with aluminum was measured using the white neutron beam of the WNR facility at the Los Alamos National Laboratory. Aluminum samples were positioned at about 20 m or 41 m distance from the neutron production target. The spectra of the emitted γ rays were measured with a high-resolution HPGe detector. The incident neutron energy was determined by the time-of-flight method and the neutron fluence was measured with a ^{238}U fission chamber. From the γ-ray spectra excitation functions for prominent γ-ray transitions in various residual nuclei (in the element range from F to Al) were derived for neutron energies from 3 to 400 MeV. Up to 200 MeV incident neutron energy the results are compared with the predictions of nuclear model calculations performed with the code GNASH. This code combines compound nucleus calculations using Hauser-Feshbach statistical theory with preequilibrium calculations from an exciton model including multiple preequilibrium processes. For the majority of the γ-ray transitions there is reasonable agreement between the measured and the calculated cross sections.
[S0556-2813(98)04404-5]

PACS number(s): 25.40.−h, 24.60.Dr

I. INTRODUCTION

One method to study neutron-induced reactions over a wide incident neutron energy range up to several hundreds of MeV is the use of a pulsed ''white'' spallation neutron source and high-resolution γ-ray spectroscopy. The incident neutron energy is determined by the time-of-flight method and the prompt γ-radiation emitted in neutron-induced reactions is detected by high-resolution Ge detectors.

In general neutron-induced reactions leave the residual nucleus in a highly excited state which subsequently decays via a γ cascade to the ground state in typically three or four steps. The initial intensity distribution over a very large number of highly exited levels is collected in the first few excited levels which then decay to the ground state. Such transitions between low-lying levels are identified in the prompt γ-ray emission-spectrum by their characteristic γ-ray energies, and production cross sections for several transitions in a number of residual nuclei can be measured simultaneously over a wide incident neutron energy range in a single experiment.

In even-even nuclei, direct transitions by particle emission to the 0^+ ground state (g.s.) are unlikely because of the many other decay modes possible. Because there is sufficient angular momentum in the system to populate a rather wide range of residual states, few of these states, except the lowest 2^+ state, decay directly to the ground state and nearly all decay through this 2^+ state. Thus the measured cross section for this $2_1^+ \rightarrow$g.s. transition is approximately equal to the total production cross section for an even-even residual nucleus. In our previous work on Pb [1] and in several of the residual nuclei here, detailed calculations show that this approximation is good to better than 90%. The partial cross section not included in this measurement results from those γ rays in the cascade which bypass the 2_1^+ state, and those reactions that leave the residual nucleus directly in the ground state.

If the residual nucleus is not even-even (or if γ-ray transitions other than the $2_1^+ \rightarrow$g.s. transition are investigated) partial production cross sections are obtained from the production cross section for a given γ-ray transition. These partial cross sections indicate the population of individual states in the same sense as the production of isomeric states and they are therefore of interest for comparison with the results of nuclear model calculations.

At the Weapons Neutron Research facility (WNR) [2] of the Los Alamos National Laboratory a program for the measurement of high-resolution γ-ray production cross sections for several elements was initiated several years ago [3]. In a collaboration between the Los Alamos National Laboratory and the University of Vienna γ-ray emission cross sections with enriched ^{207,208}Pb samples were measured and the results reported [1,4]. The main motivation for performing the present experiment was, as in the case of the lead measurement, to provide an experimental data base for comparison with the results of nuclear model calculations and to test model calculations based on the Hauser-Feshbach formalism and the exciton model for preequilibrium particle emission over a wide incident particle energy range.

Aluminum was chosen as sample material as Al is monoisotopic and thus well suited for testing model calculations. In addition there exists a good data base for proton-induced reactions on Al. The results of this work (cross section data for reactions induced by high-energy neutrons) complement the existing data base and may be used for detailed comparisons between the results of proton and neutron-induced reactions.

Furthermore, discrete γ-ray measurements are complementary to particle-emission spectra measurements, since

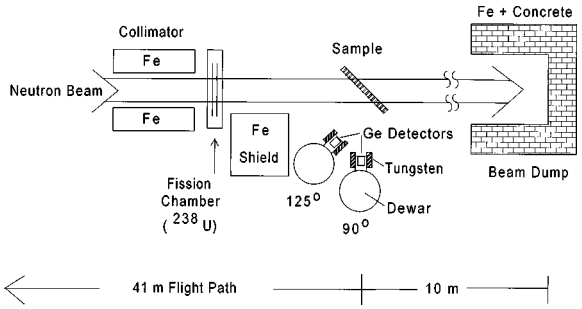

FIG. 1. Experimental setup.

they test the model's ability to predict observables sensitive to angular-momentum conservation in radionuclide production.

II. EXPERIMENT

The experimental setup was essentially the same as in the lead experiment described in Ref. [1], where a more detailed description is given. The experiments were performed at the 30° left flight path of the WNR facility. The general features of the 30° left Ge spectrometer setup and of the beam pulse structure are described in Ref. [5]. A schematic diagram of the flight path, collimation, shielding, sample position and detectors is shown in Fig. 1.

Aluminum samples were irradiated at distances of 20.06 and 41.48 m from the neutron production target. The samples were 10-cm×10-cm Al plates, 2- and 6-mm thick for the 20- and the 41-m setup, respectively. The samples were mounted on a thin plastic frame and oriented at 45° with respect to the beam to reduce the attenuation of the γ rays in the sample for detectors positioned at 90° and 125°. The collimated neutron beam was completely intercepted by the sample.

Two high-purity coaxial Ge detectors (HPGe) were used in each experiment. The detectors had active volumes of approximately 70 and 140 cm^3 for the 90° and the 125° detectors, respectively. Steel tubes filled with tungsten powder were used as collimators. As the same experimental setup was also used in a study of ^{207,208}Pb γ-ray emission spectra [1], lead could not be used as shielding material.

The detectors were positioned about 40.0 cm from the sample center at 90° and about 27 cm from the sample at 125°. The detector and collimator assemblies were positioned side by side to take advantage of the better shadow shielding on one side of the beam. The sample-to-detector distance was chosen to maximize the count rate while keeping the effects of pileup at a reasonable level for the 125° detector. The sample-to-detector distance for the 90° detector was constrained by the physical contact of the two collimators. The detector position of 125° was chosen because the value of the P_2 Legendre polynomial function is zero at that angle. The usual expansion of the γ-ray angular distribution is

$$A_0[1+a_2P_2(\cos\theta)+a_4P_4(\cos\theta)+\cdots].$$

Provided a_4 is small, the angle integrated cross section can be approximated as 4π times the measured cross section at $\theta=125°$. Data from the 90° detector were not used in the analysis or results reported in this paper. The detector efficiencies (including the solid angle) were measured by placing calibrated radioactive sources at the sample center position.

The neutron flux was measured with a fission chamber with a ^{238}U fission foil. The design of the fission chamber is described in Ref. [6]. The fission chamber was centered on the beam at distances of 19.30 and 37.30 m from the production target for the 20- and 41-m sample positions, respectively.

Data were acquired using standard electronics, a CAMAC crate and a VAXstation computer. The XSYS data acquisition and analysis computer program [7] was used. Data from the Ge detectors as well as from the fission chambers were stored in event mode on disk, and sorted into one-dimensional (1D) and 2D [neutron time-of-flight (TOF) versus pulse height] spectra. The time resolution of the 125° detector, determined from the ''γ-ray flash'' from the neutron production target varied from 10 ns full width at half maximum (FWHM) for $E_\gamma=200$ keV to 5 ns FWHM for $E_\gamma=3$ MeV. The γ-ray energy resolution obtained during the experiments was 3.9 keV FWHM at a γ-ray energy of 1014.4 keV. The γ-ray energy resolution was limited in part by the selection of a 1 μs pulse shaping time constant which allowed high count rates without excessive pileup.

To get an estimate of the γ-ray background, measurements were performed without any sample as well as with a 0.5-mm thick tantalum plate at the sample position, as a sample-out measurement does not account for background γ rays produced by neutrons which are scattered from the sample into the collimators and detectors. A significant background line interfering with the 843.7-keV $(\frac{1}{2})^+\rightarrow$g.s. transition in ^{27}Al was identified as the $2_1^+\rightarrow$g.s. 846.8-keV transition in ^{56}Fe, probably from the detector housing. Therefore the 843.7-keV transition in ^{27}Al could not be analyzed. The background spectra did not show any further γ-ray lines overlapping in energy with the γ rays of interest.

Because of uncertainty in our knowledge of the Ge detector dead time, an experiment in the 14-MeV neutron energy range was performed at the Institute of Physics of the Slovak Academy of Sciences to determine a better absolute normalization of the cross sections [8].

III. DATA REDUCTION

The neutron energy range between 3 and 400 MeV was divided into energy groups with increasing widths (0.25 to 50 MeV) according to the neutron energy resolution of the experiment.

The neutron fluence for each energy group was determined from the two dimensional (neutron TOF versus fission PH) fission chamber spectra [6]. Photofission events induced by γ rays emitted from the neutron-production target were used as a time reference to signal the arrival of the proton beam pulse at the neutron production target. The time scale was calibrated by a time calibrator with a quartz oscillator. α particles and fission fragments were distinguished by their pulse heights. A time-uncorrelated random background present in the TOF spectra was subtracted prior to sorting the fission events into neutron energy groups. The neutron fluence for each group was calculated using the cross sections for the ^{238}U(n,f) reactions given by Lisowski *et al.* [9].

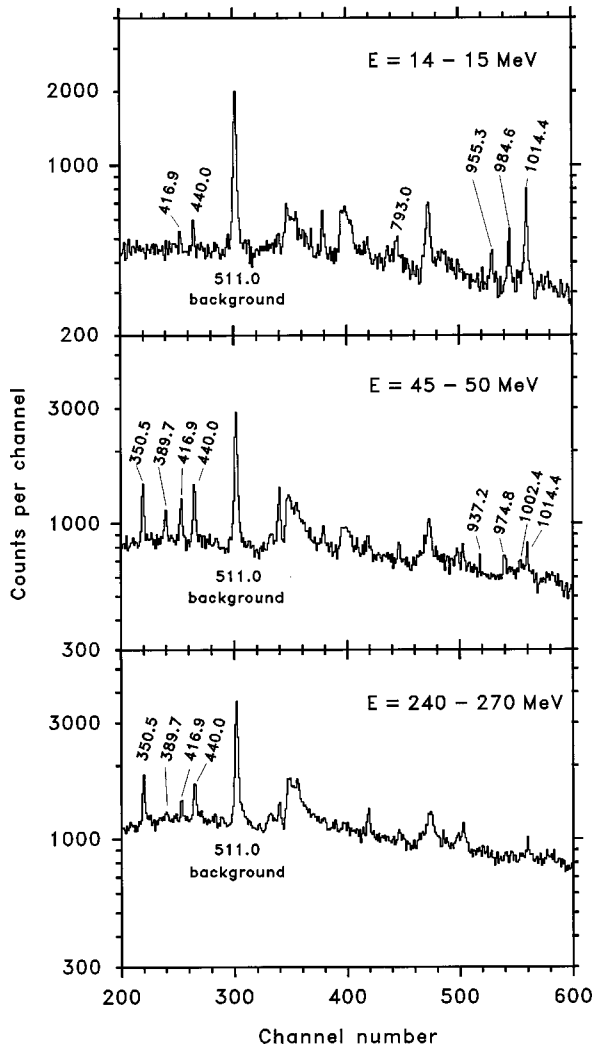

FIG. 2. γ-ray spectra derived from the data taken with the 2-mm aluminum sample for incident neutron energy groups 14 to 15 MeV, 45 to 50 MeV, and 240 to 270 MeV. The numbers in the figure are the γ-ray energies in keV of the corresponding lines, which were analyzed to derive γ-ray production cross sections.

Two-dimensional spectra, neutron TOF versus γ pulse-height, were recorded for the Ge detector. The ''γ flash'' from the neutron-production target was used as a time reference. For each neutron energy group a one-dimensional γ pulse-height spectrum was derived from the two-dimensional spectrum. Figure 2 shows examples of γ-ray spectra from the Al sample in the 20-m position for the neutron energy ranges 14 to 15 MeV, 45 to 50 MeV, and 240 to 270 MeV.

The peak areas were determined by subtracting a background interpolated linearly between suitably chosen background regions on both sides of the peak. As the choice of the peak limits and the background region is somewhat subjective, an additional uncertainty component was added quadratically to the statistical uncertainties. An estimate of this uncertainty was obtained by comparing the peak areas determined by different summing limits and background regions.

The γ-ray transitions analyzed in this work are listed in Table I. A number of γ-ray transitions originating from very short-lived levels could only be analyzed in a very restricted neutron-energy range. Due to Doppler broadening, peak areas could not be determined from the γ-ray spectra related to higher neutron-energy groups. The analyzed neutron-energy range for the 1014.4-keV transition in ^{27}Al was restricted by the contribution of multiply scattered neutrons (see below) and not by the Doppler broadening.

From the peak areas, the neutron fluence, and the γ detector efficiency, relative excitation functions were derived for each γ transition analyzed. The differential cross sections at $\theta = 125°$ were converted to total γ-production cross sections by multiplying them by 4π as discussed in Sec. II. Correction factors for the attenuation of the γ rays within the samples were calculated using photon absorption cross sections from Ref. [10].

Multiply scattered neutrons can give significant additional contributions to the measured cross sections at high incident neutron energies, especially for reactions with low thresholds. Taking into account the effect of secondary neutrons only (and neglecting higher-order multiple scattering) the correction factor for a γ-ray transition with energy E_γ at an incident neutron energy E is given by

$$f = \left(1 + \frac{N_{\rm sec}(E,E_\gamma)}{N_{\rm prim}(E,E_\gamma)} \right)^{-1}, \qquad (1)$$

where $N_{\rm prim}(E,E_\gamma)$ and $N_{\rm sec}(E,E_\gamma)$ are the γ-peak intensities due to photons produced by primary and secondary neutrons, respectively.

The ratio of the contributions of secondary and primary neutrons to the measured γ-peak intensities for a γ-ray transition with energy E_γ and a primary neutron energy E was estimated under the assumption of isotropic emission of secondary neutrons according to the relation

$$\frac{N_{\rm sec}(E,E_\gamma)}{N_{\rm prim}(E,E_\gamma)} = \frac{n\bar{l}\int_0^E \sigma_{nM}(E,E')\sigma_\gamma(E',E_\gamma)dE'}{\sigma_\gamma(E,E_\gamma)}, \qquad (2)$$

where n is the atomic density of the sample and $\bar{l}$ the average path length of the secondary neutrons in the sample, $\sigma_{nM}(E,E')$ is the energy-differential emission cross section for the production of neutrons of energy E' by neutrons of the initial energy E, and $\sigma(E,E_\gamma)$ and $\sigma(E',E_\gamma)$ are the γ-ray production cross sections for a γ-ray transition with energy E_γ at neutron energies of E and E', respectively.

The correction was done for the low-threshold reactions ^{27}Al$(n,n'\gamma)$ and ^{27}Al$(n,p\gamma)$ and could be neglected for all other reactions, as only a small fraction of the secondary neutrons had energies exceeding the reaction thresholds. The ratios $N_{\rm sec}/N_{\rm prim}$ were calculated for neutron energies of 10, 14.5, 20, 30, 40, and 60 MeV and values for intermediate energies were obtained by linear interpolation. The γ-ray production cross section used for these calculations were the results of nuclear model calculations performed with the code GNASH [11,12] in the course of this work (see Sec. IV). For the neutron emission cross sections experimental data were used for $E = 14.5$ MeV [13], for $E = 10$ and 20 MeV we used evaluated values from the JENDL-3 library [14] and for the higher neutron energies we used the results of the present model calculations with the code GNASH. An estimated uncertainty of $\pm 30\%$ was assigned to the calculated $N_{\rm sec}/N_{\rm prim}$ ratios. Due to the lower production cross sections for protons and the smaller range due to slowing down, contributions of secondary protons to the measured cross sections can be ex-

TABLE I. Nuclear reactions and γ transitions investigated in this work.

Reaction	Residual nucleus	γ Transition investigated	Energy (keV)	Neutron energy range (MeV)
^{27}Al($n,n'\gamma$)	^{27}Al	$9/2^+ \rightarrow 7/2^+$	793.0	3–26
		$3/2^+ \rightarrow$g.s.	1014.4	3–60
		$5/2^+ \rightarrow 3/2^+$	1720.3	3–12
		$7/2^+ \rightarrow$g.s.	2211.1	3–34
		$9/2^+ \rightarrow$g.s.	3004.2[a]	3–20
^{27}Al($n,2n\gamma$)	^{26}Al	$3^+ \rightarrow$g.s.	416.9	threshold–400
		$1^+ \rightarrow 0^+$	829.4	threshold–40
^{27}Al($n,p\gamma$)	^{27}Mg	$5/2^+ \rightarrow 3/2^+$	955.3	threshold–19
		$3/2^+ \rightarrow$g.s.	984.6	threshold–32
		$5/2^+ \rightarrow$g.s.	1697.9	threshold–32
^{27}Al($n,pn\gamma$) ^{27}Al($n,d\gamma$)	^{26}Mg	$3_1^+ \rightarrow 2_1^+$	1002.4	threshold–60
		$2_2^+ \rightarrow 2_1^+$	1129.7	threshold–400
		$2_1^+ \rightarrow$g.s.	1808.6	threshold–400
^{27}Al($n,p2n\gamma$)	^{25}Mg	$3/2^+ \rightarrow 1/2^+$	389.7	threshold–400
^{27}Al($n,dn\gamma$)		$3/2^+ \rightarrow$g.s.	974.8	threshold–400
^{27}Al($n,p3n\gamma$) ^{27}Al($n,d2n\gamma$)	^{24}Mg	$2^+ \rightarrow$g.s.	1368.6	threshold–400
^{27}Al($n,2p3n\gamma$) ^{27}Al($n,\alpha n\gamma$)	^{23}Na	$5/2^+ \rightarrow$g.s.	440.0	threshold–400
^{27}Al($n,3p3n\gamma$) ^{27}Al($n,\alpha pn\gamma$)	^{22}Ne	$2^+ \rightarrow$g.s.	1274.5	threshold–400
^{27}Al($n,3p4n\gamma$) ^{27}Al($n,\alpha p2n\gamma$)	^{21}Ne	$5/2^+ \rightarrow$g.s.	350.5	threshold–400
^{27}Al($n,3p5n\gamma$) ^{27}Al($n,\alpha p3n\gamma$)	^{20}Ne	$2^+ \rightarrow$g.s.	1633.8	threshold–400
^{27}Al($n,4p6n\gamma$) ^{27}Al($n,\alpha 2p4n\gamma$) ^{27}Al($n,2\alpha 2n\gamma$)	^{18}F	$3^+ \rightarrow$g.s.	937.2	threshold–400

[a]This line was not resolved from the 2981.8-keV ($3/2^+ \rightarrow$g.s.) transition due to Doppler broadening.

pected to be at least one order of magnitude smaller than the effect of secondary neutrons. Thus such corrections were neglected.

In the case of the residual nucleus ^{27}Al we used only the data taken with the 2-mm thick sample in the 20-m sample position as for the 6-mm sample the correction factors could only be estimated with high uncertainties. For the 1014.4-keV $3/2^+ \rightarrow$g.s. transition in ^{27}Al we determined cross sections only up to a neutron energy of 60 MeV, where the correction factor reached a value of 0.50. For the other transitions in ^{27}Al the neutron energy range was restricted by the effect of Doppler broadening of the γ peaks. At the maximum neutron energies the correction factors were between 0.83 and 0.97 for the transitions analyzed.

For the residual nucleus ^{27}Mg, which is produced by the (n,p) reaction, the correction factors for the contribution of secondary neutrons are much smaller due to the higher effective reaction threshold. Therefore we estimated the correction factors for both the 2- and the 6-mm thick sample. For the highest neutron energies considered, the correction factors for the three analyzed transitions were in the range 0.87 to 0.97 for the 2-mm sample and in the range 0.70 to 0.95 for the 6-mm sample.

Because of uncertainty in our knowledge of the Ge detector dead time, the measured (relative) cross sections were normalized to data obtained in a separate measurement performed at the Institute of Physics of the Slovak Academy of Sciences in Bratislava with an incident neutron energy of 14.6 MeV [8]. For the experiment in the 41-m sample position a normalization factor was derived from the cross section of the 1808.6-keV $2_1^+ \rightarrow$g.s. transition in ^{26}Mg and for the 20-m sample position from the cross sections of the 1808.6-keV $2_1^+ \rightarrow$g.s. transition in ^{26}Mg and the 1014.4-keV $3/2^+ \rightarrow$g.s. and the 2211.1-keV $7/2^+ \rightarrow$g.s. transitions in ^{27}Al.

For ^{27}Al the final results are the normalized results from the 20-m sample position, for all other residual nuclei the final result was calculated as a weighted average of the normalized cross sections measured at the 20- and 41-m sample positions.

To estimate the final uncertainties of the γ production cross sections, all statistical and systematic uncertainty components were combined according to the rules of error propagation.

IV. CROSS SECTION CALCULATIONS

Calculations of the measured γ-ray production cross sections were performed with the reaction theory code GNASH [11,12]. GNASH combines compound nucleus calculations us-

ing Hauser-Feshbach statistical theory with preequilibrium calculations from an internal exciton model and direct reaction components from external calculations. Transmission coefficients for light particles are obtained from optical model potentials, and γ-ray transmission coefficients are calculated from a giant-dipole-resonance model by Kopecky and Uhl [15]. The structure of residual nuclei in the calculations is obtained from experimental information on discrete levels matched to phenomenological level density expressions, which are used in the continuum region.

The GNASH code is perhaps unique among existing nuclear model codes in that it applies the Hauser-Feshbach (and not Weisskopf-Ewing) theory up to incident energies as high as 200 MeV for all decaying compound nuclei, an essential prerequisite for analyzing our γ-ray data.

Particle transmission coefficients were calculated with the SCAT2 code [16] using spherical optical model potentials. For neutrons, the potential of Petler *et al.* [17], derived from $n + {}^{27}$Al scattering and total cross section measurements, was utilized for energies to 60 MeV. For protons, the global potential of Perey [18] was used to proton energies of 44 MeV, and for both neutrons and protons, the potential of Madland [19] was used at higher energies. For deuterons, the potential of Perey and Perey [20] was used at all energies, and for tritons, the Becchetti and Greenlees potential [21] was adopted. Finally, the potential of Arthur and Young [22], based on the work of Lemos [23], was used at all α energies.

Information on discrete levels (energies, spins, parities, and branching ratios) was taken from the ENSDF nuclear structure data file, which in this mass range is based mainly on the compilations of Endt [24]. The number of discrete levels and the corresponding excitation energy ranges for the various residual nuclei in the calculations are given in Table II. The phenomenological model of Ignatyuk [25] was used to calculate level densities in the continuum region. In addition to including an energy-dependent level density parameter, the Ignatyuk model accounts for the theoretically expected disappearance of shell effects in the nuclear level densities at higher excitation energies. Within this model the nuclear moment of inertia was given the full rigid body moment of inertia. The level density parameters were chosen using the systematics of Young *et al.* [26], and adjustments were made to the pairing energies based on measurements of $(n,2n)$ cross sections near threshold for the various isotopes of Al.

Preequilibrium calculations were carried out with the exciton model of Kalbach [27], including both surface effects [28] and multiple preequilibrium processes. The damping matrix element was taken as 140 MeV^3. The importance of multiple preequilibrium effects for calculating $(n,x\gamma)$ cross sections at higher energies was established in a previous analysis [1] of ^{207,208}Pb$(n,x\gamma)$ reactions. Calculations using the GNASH code are shown in Figs. 3–13 for two different options for modeling multiple preequilibrium emission: our earlier [1] model (MPE1), which determines the emission of a second preequilibrium particle from the dominant $1p1h$ states using an exciton model; and our more recent [29] generalized multiple preequilibrium model (MPE2), which determines second-particle emission from all preequilibrium particle-hole states. Comparisons of the predictions from these models with experimental emission spectra data [30] indicate a preference for the more recent model (MPE2). This is because particle emission at medium to low emission energies, but above the evaporation regime, is more properly accounted for with MPE2 by second-particle preequilibrium emission from the more complex particle-hole states.

TABLE II. Maximum excitation energies and numbers of discrete states included for various residual nuclei in the ^{27}Al$+n$ calculations.

Residual nucleus	Maximum excitation energy (MeV)	Number of discrete states
^{28}Al	4.081	28
^{27}Al	7.012	41
^{26}Al	5.522	53
^{25}Al	5.609	25
^{24}Al	4.025	13
^{23}Al	0.000	1
^{22}Al	0.000	1
^{27}Mg	5.244	20
^{26}Mg	6.945	20
^{25}Mg	5.319	20
^{24}Mg	9.534	27
^{23}Mg	6.200	20
^{22}Mg	6.036	12
^{26}Na	2.539	8
^{25}Na	5.043	20
^{24}Na	3.694	20
^{23}Na	6.079	20
^{22}Na	4.522	20
^{21}Na	5.834	20
^{20}Na	0.000	1
^{25}Ne	0.000	1
^{24}Ne	4.947	6
^{23}Ne	4.021	14
^{22}Ne	7.126	20
^{21}Ne	5.694	20
^{20}Ne	5.866	6
^{19}Ne	3.385	7
^{22}F	0.000	1
^{21}F	5.091	20
^{20}F	4.141	20
^{19}F	5.516	20
^{18}F	4.803	20
^{17}F	0.000	1
^{16}F	0.000	1

V. RESULTS AND DISCUSSION

The results of this work, the measured and calculated excitation functions of 21 transitions between low-lying levels in 11 different residual nuclei, are given in Figs. 3–13. Numerical values of the experimental results are available in EXFOR format through the Nuclear Data Centers [31]. An overview of the analyzed transitions and the neutron energy ranges where cross sections could be determined is given in Table I. All experimental results are normalized to the results of the 14-MeV experiment (see Sec. III). We note, that the

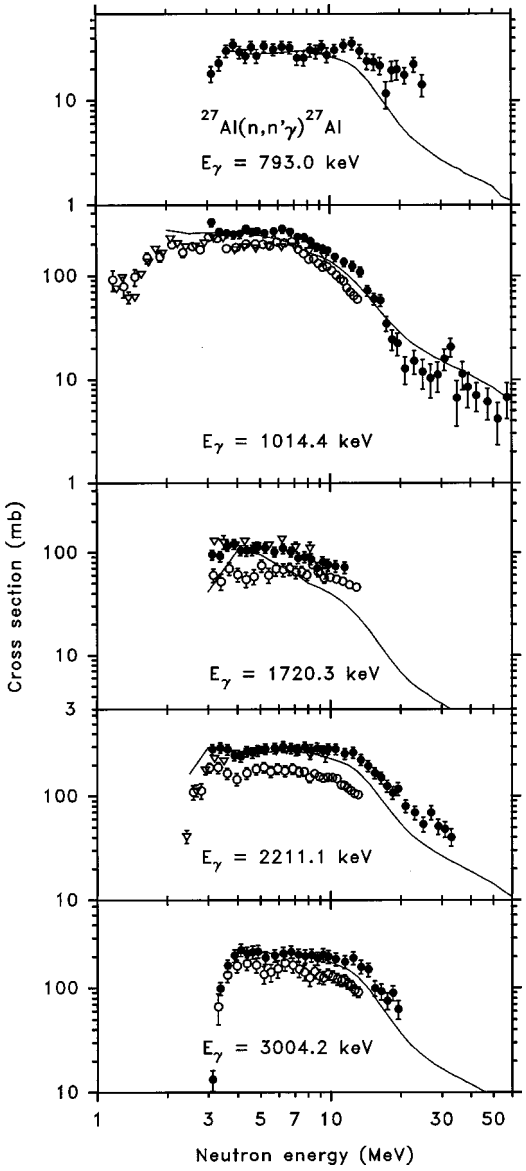

FIG. 3. ^{27}Al($n,n'\gamma$)^{27}Al cross sections for the transitions with 793.0, 1014.4, 1720.3, 2211.1, and 3004.2 keV γ-ray energy in ^{27}Al. Closed circles: present experiment. Solid line: GNASH calculations (No difference between MPE1 and MPE2.) Open circles: Voss *et al.* [32]. Open triangles: Savin *et al.* [33].

relative intensities for the various cross sections measured at $E_n = 14$ MeV in the present experiment agree within the uncertainty limits with the results of the independently performed 14-MeV experiment.

γ-ray production cross sections from the interaction of fast neutrons with aluminum were measured previously with high resolution in the energy ranges 0.8 to 13 MeV [32] and 0.8 to 10 MeV [33] and for neutron energies around 14 MeV. A detailed discussion of the widely discrepant 14-MeV measurements is given in Ref. [8] and is therefore not repeated here. The results of Voss *et al.* [32] and Savin *et al.* [33] who had studied transitions in ^{27}Al only are included in Fig. 3. The results given by Voss *et al.* [32] are about 30% lower than our measurements indicating differences in the absolute normalization. The cross sections given by Savin *et al.* show rather good agreement with our own data for the 1720.3-keV and the 2211.1-keV transition in ^{27}Al, but are about 30%

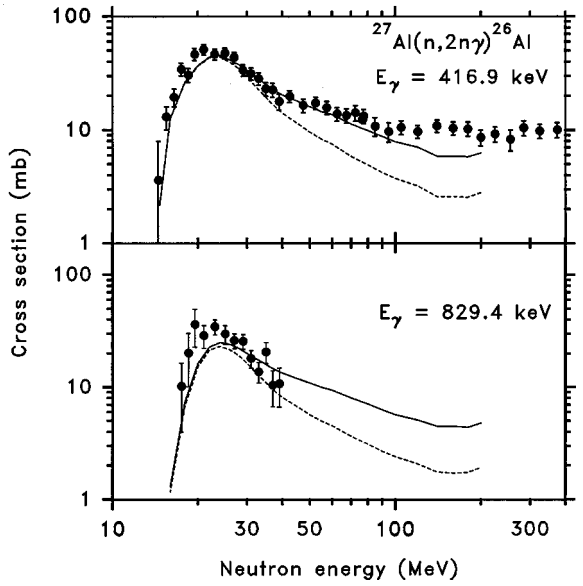

FIG. 4. ^{27}Al($n,2n\gamma$)^{26}Al cross sections for the transitions with 416.9 and 829.4 keV γ-ray energy in ^{26}Al. Closed circles: present experiment. Solid line: GNASH calculations (MPE1). Dashed line: GNASH calculations (MPE2).

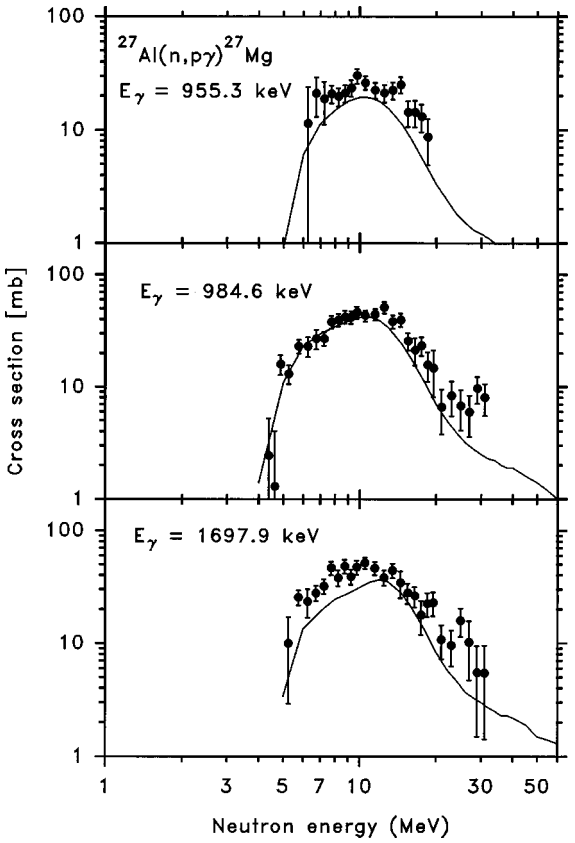

FIG. 5. ^{27}Al($n,p\gamma$)^{27}Mg cross sections for the transitions with 955.3, 984.6, and 1697.9 keV γ-ray energy in ^{27}Mg. Closed circles: present experiment. Solid line: GNASH calculations (No difference between MPE1 and MPE2.)

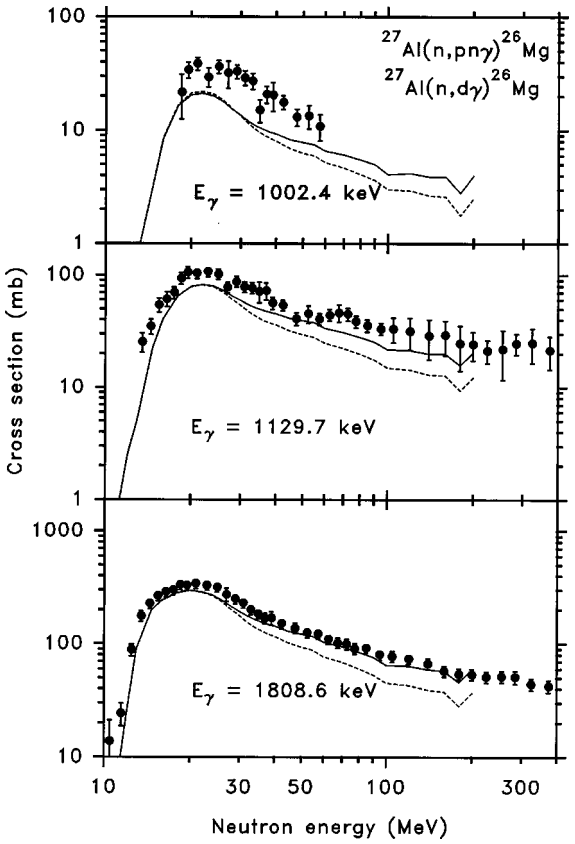

FIG. 6. Sum of the ^{27}Al$(n,pn\gamma)^{26}$Mg and ^{27}Al$(n,d\gamma)^{26}$Mg cross sections for the transitions with 1002.4, 1129.7, and 1808.6 keV γ-ray energy in ^{26}Mg. Closed circles: present experiment. Solid line: GNASH calculations (MPE1). Dashed line: GNASH calculations (MPE2).

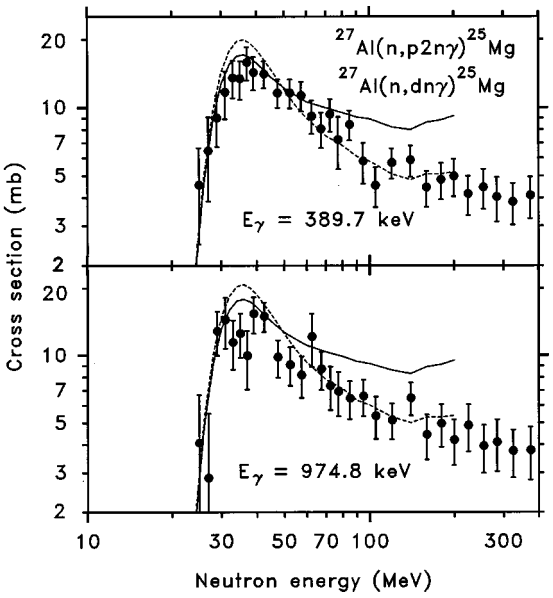

FIG. 7. Sum of the ^{27}Al$(n,p2n\gamma)^{25}$Mg and ^{27}Al$(n,dn\gamma)^{25}$Mg cross sections for the transitions with 389.7 and 974.8 keV γ-ray energy in ^{25}Mg. Closed circles: present experiment. Solid line: GNASH calculations (MPE1). Dashed line: GNASH calculations (MPE2).

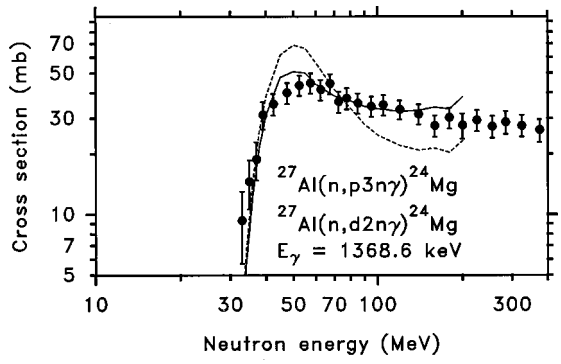

FIG. 8. Sum of the ^{27}Al$(n,p3n\gamma)^{24}$Mg and ^{27}Al$(n,d2n\gamma)^{24}$Mg cross sections for the 1368.6-keV transition in ^{24}Mg. Closed circles: present experiment. Solid line: GNASH calculations (MPE1). Dashed line: GNASH calculations (MPE2).

lower for the 1014.4-keV transition. Such differences in the relative intensities of transitions in the same residual nucleus are difficult to understand as all normalization factors and also corrections for finite sample-size effects should be approximately the same.

In Figs. 3–13 the results of the model calculation (see Sec. IV) with the GNASH code using both models for multiple preequilibrium particle emission (MPE1 and MPE2) are shown. There are no differences in the results for the two models for the $(n,n'\gamma)$ and the $(n,p\gamma)$ reactions (Figs. 3 and 5). For these reactions the model calculations give a reasonable reproduction of the experimental cross sections with deviations of about 20% which are to be expected for such calculations.

The importance of the chosen multiple preequilibrium model can be seen in the other figures, where differences in the calculated γ-ray cross sections (and radionuclide yields) for the two models are seen in some cases to be large, particularly for the $(n,2n\gamma)$ cross sections (Fig. 4). This is to be expected since the $(n,2n)$ cross section is particularly sensitive to reaction mechanisms which result in the emission of two fast particles, leaving the residual nucleus in a low excitation state. In Fig. 4 it is evident that both the MPE1 and MPE2 model calculations are in reasonable agreement with the $(n,2n\gamma)$ data for the 829.4-keV transition, but the MPE2 calculation underpredicts the measurement for the 416.9-keV

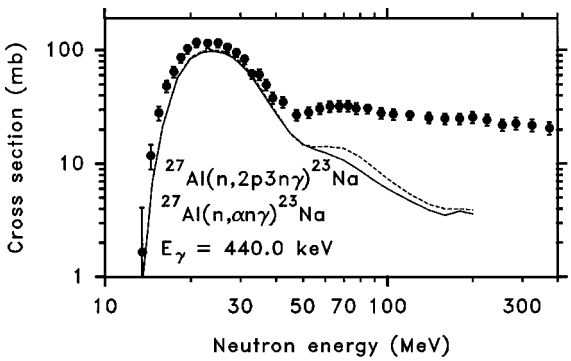

FIG. 9. Sum of the ^{27}Al$(n,2p3n\gamma)^{23}$Na and ^{27}Al$(n,\alpha n\gamma)^{23}$Na cross sections for the 440.0-keV transition in ^{23}Na. Closed circles: present experiment. Solid line: GNASH calculations (MPE1). Dashed line: GNASH calculations (MPE2).

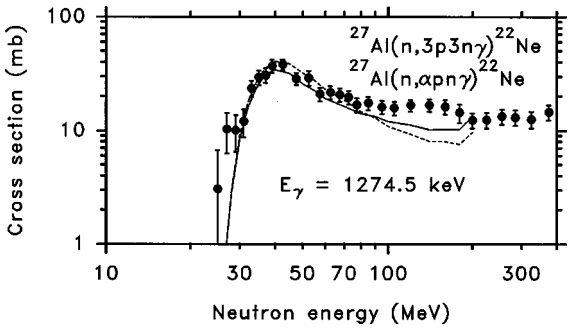

FIG. 10. Sum of the ^{27}Al($n,3p3n\gamma$)^{22}Ne and ^{27}Al($n,\alpha pn\gamma$)^{22}Ne cross sections for the 1274.5-keV transition in ^{22}Ne. Closed circles: present experiment. Solid line: GNASH calculations (MPE1). Dashed line: GNASH calculations (MPE2).

transition above 40 MeV. Possible reasons for the underprediction by the MPE2 model calculation are discussed in more detail below.

For the ($n,pn\gamma$) cross section (Fig. 6) the model calculation results using MPE2 again underestimate the measured cross sections. For the 1002.4-keV transition there is a general disagreement of about a factor 2 between the experimental and the calculated γ-ray production cross sections. The structures in the calculated cross section curves for neutron energies above 150 MeV are caused by the numerical procedures and can be removed at the expense of more computing resources. In the case of the ($n,p2n\gamma$) and ($n,p3n\gamma$) reactions (Figs. 7 and 8) the calculations using MPE2 give higher cross sections in the peak region of the excitation function than our original preequilibrium model (MPE1) but they are lower for higher energies. The MPE2 calculations give a better reproduction of the experimental data for the ($n,p2n\gamma$) reaction, whereas for the ($n,p3n\gamma$) reaction the MPE1 results agree with the experimental cross sections. In the case of the γ-ray production cross section for the 440.0-keV transition in ^{23}Na (Fig. 9), both preequilibrium models give similar results which show a strong disagreement with the experimental data for neutron energies above 40 MeV. The observed shape of the measured excitation function of the 440-keV γ ray in ^{23}Na is due to two main reaction channel contributions: at the lowest energies, with a threshold energy of approximately 10.5 MeV, is a contribution involving α-particle emission [($n,n\alpha$) and ($n,\alpha n$) channels]; at higher energies, with a threshold of approximately 40 MeV,

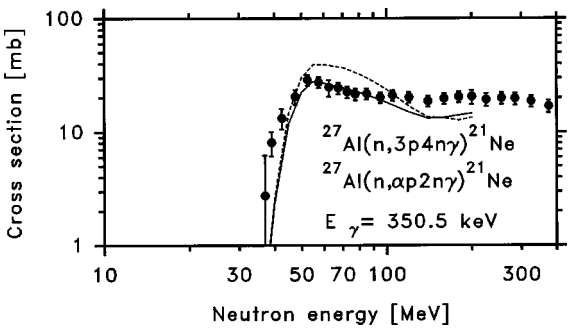

FIG. 11. Sum of the ^{27}Al($n,3p4n\gamma$)^{21}Ne and ^{27}Al($n,\alpha p2n\gamma$)^{21}Ne cross sections for the 350.5-keV transition in ^{21}Ne. Closed circles: present experiment. Solid line: GNASH calculations (MPE1). Dashed line: GNASH calculations (MPE2).

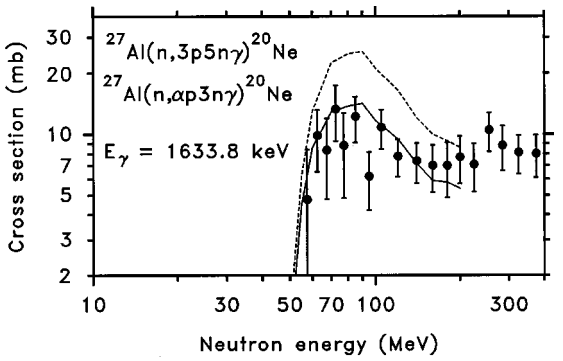

FIG. 12. Sum of the ^{27}Al($n,3p5n\gamma$)^{20}Ne and ^{27}Al($n,\alpha p3n\gamma$)^{20}Ne cross sections for the 1633.8-keV transition in ^{20}Ne. Closed circles: present experiment. Solid line: GNASH calculations (MPE1). Dashed line: GNASH calculations (MPE2).

is a contribution from the sequential emission of three neutrons and two protons. While the calculations account for the former mechanism, they underpredict the latter reaction channel. This is due to the calculations predicting the presence of other competing decay channels that take away cross section from this channel. While we could have modified input model parameters (particularly level density parameters) to enhance this decay channel and obtain an improved agreement with the measurements, we did not do this because of the advantages of presenting results of model calculations using default input parameters.

For the γ-ray production cross sections of transitions in ^{22}Ne and ^{21}Ne (Figs. 10 and 11) the calculations using both preequilibrium models result in very similar excitation functions. The overall agreement seems to be somewhat better using the MPE1 model. For the 1633.8-keV γ-ray transition in ^{20}Ne (Fig. 12) there is good agreement (within the experimental uncertainties) between the experimental cross sections and the calculations using MPE1. The results obtained with MPE2 overestimate the measured cross sections. For the γ-ray production cross section of the 937.2-keV transition in ^{18}F (Fig. 13) there is disagreement between the GNASH calculations and the measured cross sections in the neutron energy range between threshold and about 60 MeV. This discrepancy is not yet understood.

As already mentioned in Sec. IV the more recent preequilibrium model (MPE2) uses more realistic assumptions on

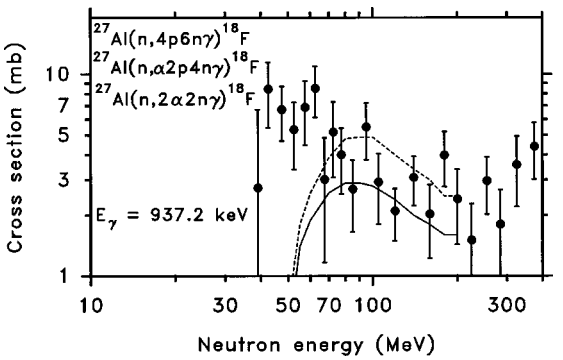

FIG. 13. Sum of the ^{27}Al($n,4p6n\gamma$)^{18}F, ^{27}Al($n,\alpha 2p4n\gamma$)^{18}F, and ^{27}Al($n,2\alpha 2n\gamma$)^{18}F cross sections for the 937.2-keV transition in ^{18}F. Closed circles: present experiment. Solid line: GNASH calculations (MPE1). Dashed line: GNASH calculations (MPE2).

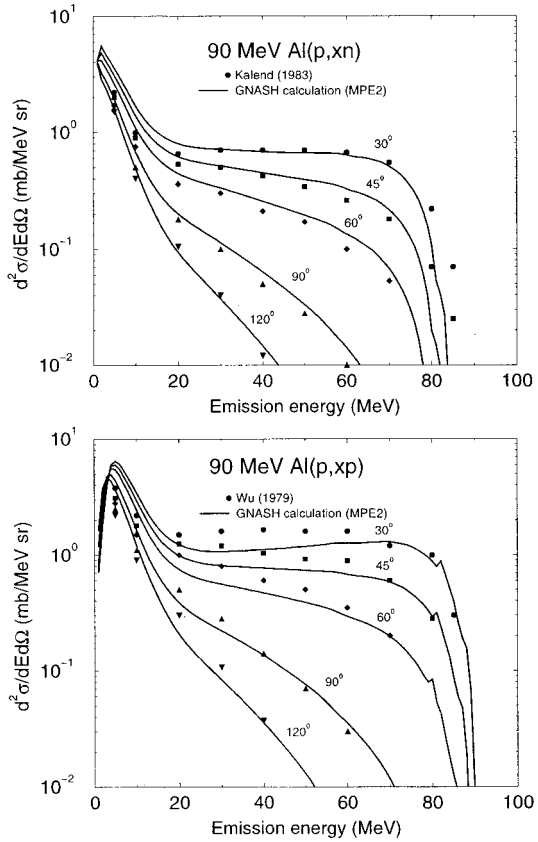

FIG. 14. Proton and neutron emission spectra in the 90-MeV $p+\mathrm{Al}$ reaction. Solid line: GNASH calculations (MPE2 models). Symbols: Experimental (p,xn) data of Kalend *et al.* [34] (upper figure); experimental (p,xp) data of Wu *et al.* [35] (lower figure).

the emission of the second preequilibrium particle than the original one (MPE1). To better understand the role of multiple preequilibrium reactions, we show the calculated angle-integrated neutron and proton emission spectra following 90-MeV protons incident on Al, compared to the data of Kalend *et al.* [34] and Wu *et al.* [35] in Fig. 14 (such data for incident neutrons do not exist). Angular distributions for the secondary ejectiles in the calculations were obtained using the Kalbach systematics [36], and the results transformed into the laboratory frame assuming two-body kinematics. In fact, the forward-peaking exhibited in the evaporation regime, which comes from the center-of-mass system to laboratory system transformation, is an artifact due to this assumption. In reality, the preequilibrium ejectiles, which are generally emitted with high energy in the forward direction, lead to a

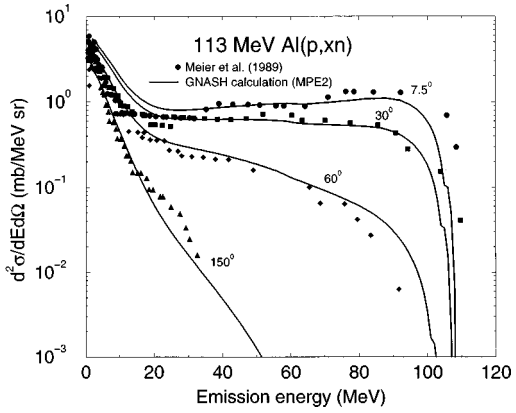

FIG. 15. Neutron emission spectra in the 113 MeV $p+\mathrm{Al}$ reaction. Solid line: GNASH calculations (MPE2). Symbols: Experiment of Meier *et al.* [37].

significant decrease in the kinetic energy of the decaying compound nuclei, so that the transformation into the laboratory frame should not lead to much forward-peaking in the evaporation region. The GNASH model calculations (which use the preferred MPE2 model) are seen to describe the data fairly well, though the forward-angle proton spectra are underpredicted by approximately 20–30 %. Likewise, Fig. 15 shows the Los Alamos Meier *et al.* [37] data for the 113-MeV Al(p,xn) reaction compared with our calculations, and again the agreement between calculation and measurement is good. But these figures do show a tendency for an overprediction of evaporation neutrons and protons, which suggests that the calculated preequilibrium emission may be underestimated (more high-energy ejectiles leave less energy for sequential equilibrium decays). However, with the exception of the 90-MeV proton emission spectrum, the preequilibrium spectra appear to be described well with the GNASH MPE2 model.

Table III shows that the calculated integrated cross sections for secondary particle production for various emission mechanisms agree well with the Wu *et al.* data [35] for 90-MeV $p+\mathrm{Al}$. The good agreement between theory and experiment for proton emission may be somewhat fortuitous, since Fig. 14 suggests that a theoretical underprediction in preequilibrium emission is compensated by an overprediction in equilibrium emission. The importance of preequilibrium deuteron emission, which is included in our calculations, is also evident.

Given the reasonably good description of emission spectra obtained with MPE2, described above, how can the MPE2 model's failure to describe the measured $(n,2n\gamma)$

TABLE III. Secondary particle production (in mb) for the 90-MeV $p+\mathrm{Al}$ reaction, compared with experimental results of Wu *et al.* [35].

	GNASH Calculations (MPE2)				
Ejectile	Primary preequilibrium	Multiple preequilibrium	Evaporation	Total	Experiment (Wu *et al.*) Total
n	118	75	254	447	
p	245	87	426	758	723
d	64	0	23	87	93
α	8	0	132	140	161

(E_γ=416.9 keV) cross section above 50 MeV be understood? Since the multiple preequilibrium model is statistical in nature, and the processes that contribute to the ($n,2n\gamma$) cross section are only a small subset of all the multiple emission processes observed in the emission spectra, perhaps the ($n,2n$) reaction is particularly sensitive to nuclear structure details and would be better described by a knockout distorted-wave reaction theory.

A final piece of evidence that is relevant to this discussion is measurements of radionuclide production cross sections in proton-induced reactions, by Michel and collaborators [38,39], and by Sisterson *et al.* [40]. For the $p+^{27}$Al reaction at 90 MeV (one of the incident energies discussed above), these authors measure radionuclide production cross sections of approximately: ($p,pn+d$) ^{26}Al production: 52 mb (GNASH predicts 60 mb); ($p,3pn$) ^{24}Na production: 11 mb (GNASH predicts 9 mb); and ($p,3p3n$) ^{22}Na: 21 mb (GNASH predicts 21 mb). Thus, excellent agreement is obtained between GNASH, using MPE2, and the experimental data. In particular, the (p,pn) cross section comparison, which is particularly sensitive to multiple preequilibrium modeling, supports the applicability of the MPE2 GNASH model, in contrast to our present ($n,2n\gamma$) measurements.

[1] H. Vonach, A. Pavlik, M. B. Chadwick, R. C. Haight, R. O. Nelson, S. A. Wender, and P. G. Young, Phys. Rev. C **50**, 1952 (1994).

[2] P. W. Lisowski, C. D. Bowman, G. J. Russell, and S. A. Wender, Nucl. Sci. Eng. **106**, 208 (1990).

[3] R. O. Nelson, S. A. Wender, and D. R. Mayo, ''Gamma-ray measurements at the WNR white neutron source,'' in *Proceedings of a Specialists' Meeting on Measurement, Calculation and Evaluation of Photon Production Data*, edited by C. Coceva, A. Mengoni, and A. Ventura, Bologna, Italy, 1994, Nuclear Energy Agency Report No. NEA/NSC/DOC(95)1, Bologna, 1995, p. 281.

[4] A. Pavlik, H. Vonach, R. O. Nelson, R. C. Haight, S. A. Wender, P. G. Young, and M. B. Chadwick, International Nuclear Data Committee Report No. INDC(NDS)-334, Vienna, 1995, p. 39.

[5] R. O. Nelson, C. M. Laymon, and S. A. Wender, Nucl. Instrum. Methods Phys. Res. B **56**, 451 (1991).

[6] S. A. Wender, S. Balestrini, A. Brown, R. C. Haight, C. M. Laymon, T. M. Lee, P. Lisowski, W. McCorkle, R. O. Nelson, and W. Parker, Nucl. Instrum. Methods Phys. Res. A **336**, 226 (1993).

[7] N. R. Yoder, Indiana University Cyclotron Facility internal report, 1991.

[8] S. Hlaváč, L. Dostál, I. Turzo, A. Pavlik, and H. Vonach, Nucl. Sci. Eng. **125**, 196 (1997).

[9] P. W. Lisowski, A. Gavron, W. E. Parker, J. L. Ullmann, S. J. Balestrini, A. D. Carlson, O. A. Wasson, and N. W. Hill, ''Fission Cross Sections in the Intermediate Energy Region,'' in *Proceedings of the Specialists' Meeting on Neutron Cross Section Standards for the Energy Region above 20 MeV*, Uppsala, Sweden, 1991, Nuclear Energy Agency Nuclear Data Committee Report No. NEANDC-305 '*U*', Paris, 1991, p. 177.

[10] XRAY—The evaluated photoatomic interaction data file, data received from IAEA Nuclear Data Section, 1995.

[11] P. G. Young, E. D. Arthur, and M. B. Chadwick, ''Comprehensive Nuclear Model Calculations: Theory and Use of the GNASH Code,'' in Nuclear Reaction Data and Nuclear Reactors: Physics, Design and Safety (Lecture Series 1996, Trieste, Italy), edited by A. Gandini and G. Reffo (World Scientific, Singapore, 1998).

[12] P. G. Young, E. D. Arthur, and M. B. Chadwick, Los Alamos National Laboratory Report No. LA-12343-MS, 1992.

[13] A. Takahashi, E. Ichimura, Y. Sasaki, and H. Sugimoto, Osaka University Intense Neutron Source Facility Report No. OKTAVIAN A-87-03, Osaka, 1987, Vol. 1.

[14] JENDL-3, The Japanese Evaluated Neutron Data Library, data received from IAEA Nuclear Data Section, 1995.

[15] J. Kopecky and M. Uhl, Phys. Rev. C **42**, 1941 (1990).

[16] O. Bersillon, Commissariat à l'Energie Atomique Report No. CEA-N-2037, Bruyeres-le-Chatel, 1978, p. 111.

[17] J. S. Petler, M. S. Islam, R. W. Finlay, and F. S. Dietrich, Phys. Rev. C **32**, 673 (1985).

[18] F. G. Perey, Phys. Rev. **131**, 745 (1963).

[19] D. G. Madland, ''Recent Results in the Development of a Global Medium-Energy Nucleon-Nucleus Optical-Model Potential,'' in *Proceedings of the Specialists' Meeting on Preequilibrium Nuclear Reactions*, Semmering, Austria, 1988, edited by B. Strohmaier, Nuclear Energy Agency Nuclear Data Committee Report No. NEANDC-245 '*U*', Paris, 1988, p. 103.

[20] C. M. Perey and F. G. Perey, Phys. Rev. **132**, 755 (1963).

[21] F. D. Becchetti, Jr. and G. W. Greenlees, in *Polarization Phenomena in Nuclear Reactions*, edited by H. H. Barschall and W. Haeberli (The University of Wisconsin Press, Madison, 1971), p. 682.

[22] E. D. Arthur and P. G. Young, ''Evaluation of Neutron Cross Sections to 40 MeV for ^{54,56}Fe,'' *Proceedings of the Symposium on Neutron Cross Sections from 10 to 50 MeV*, Brookhaven National Laboratory, Upton, N.Y., 1980, edited by M. R. Bhat and S. Pearlstein, Brookhaven National Laboratory Report No. BNL-NCS-51245, 1980, Vol. II, p. 731; Los Alamos National Laboratory Report No. LA-8626-MS, 1980.

[23] O. F. Lemos, Orsay Report, Series A, No. 136, 1976.

[24] P. M. Endt, Nucl. Phys. **A521**, 1 (1990).

[25] A. V. Ignatyuk, G. N. Smirenkin, and A. S. Tishin, Yad. Fiz. **21**, 485 (1975) [Sov. J. Nucl. Phys. **21**, 255 (1975)].

[26] P. G. Young, E. D. Arthur, M. Bozoian, T. R. England, G. M. Hale, R. J. LaBauve, R. C. Little, R. E. MacFarlane, D. G. Madland, R. T. Perry, and W. B. Wilson, Trans. Am. Nucl. Soc. **60**, 271 (1989); Los Alamos National Laboratory Report No. LA-11753-MS, 1990.

[27] C. Kalbach, Z. Phys. A **283**, 401 (1977).

[28] C. Kalbach, Phys. Rev. C **32**, 1157 (1985).

[29] M. B. Chadwick, P. G. Young, D. C. George, and Y. Watanabe, Phys. Rev. C **50**, 996 (1994).

[30] M. B. Chadwick and P. G. Young, Lawrence Livermore National Laboratory informal Report No. UCRL-ID-118720, 1994.

[31] A. Pavlik, H. Hitzenberger-Schauer, H. Vonach, M. B. Chadwick, R. C. Haight, R. O. Nelson, and P. G. Young, CSISRS

Data Library, Entry No. 13643, Brookhaven National Laboratory, 1997.

[32] F. Voss, S. Cierjacks, and L. Kropp, ''Measurement of High Resolution γ-ray Production Cross Sections in Inelastic Neutron Scattering on Al and Fe Between 0.8–13 MeV,'' *Proceedings of the Third Conference on Neutron Cross Sections and Technology*, Knoxville, Tennessee, 1971, Report CONF-710301, 1971, Vol. 1, p. 218.

[33] M. V. Savin, Yu. A. Khokhlov, I. N. Paramonova, V. A. Chirkin, V. N. Ludin, M. K. Saraeva, and V. A. Zherebtsov, Yad. Fiz. **23**, 512 (1976) [Sov. J. Nucl. Phys. **23**, 269 (1976)].

[34] A. M. Kalend *et al.*, Phys. Rev. C **28**, 105 (1983).

[35] J. R. Wu, C. C. Chang, and H. D. Holmgren, Phys. Rev. C **19**, 698 (1979).

[36] C. Kalbach, Phys. Rev. C **37**, 2350 (1988).

[37] M. M. Meier, D. A. Clark, C. A. Goulding, J. B. McClelland, G. L. Morgan, and C. E. Moss, Nucl. Sci. Eng. **102**, 310 (1989).

[38] R. Michel, R. Bodemann, H. Busemann, R. Daunke, M. Gloris, H.-J. Lange, B. Klug, A. Krins, I. Leya, M. Lüpke, S. Neumann, H. Reinhardt, M. Schnatz-Büttgen, U. Herpers, Th. Schiekel, F. Sudbrock, B. Holmqvist, H. Condé, P. Malmborg, M. Suter, B. Dittrich-Hannen, P.-W. Kubik, and H.-A. Synal, Nucl. Instrum. Methods Phys. Res. B **129**, 153 (1997).

[39] R. Bodemann, H.-J. Lange, R. Michel, T. Schiekel, R. Rösel, U. Herpers, H.-J. Hofmann, B. Dittrich, M. Suter, W. Wölfli, B. Holmqvist, H. Condé, and P. Malmborg, Nucl. Instrum. Methods Phys. Res. B **82**, 9 (1993).

[40] J. M. Sisterson, K. Kim, A. Beverding, P. A. J. Englert, M. W. Caffee, J. Vincent, C. Castenada, and R. C. Reedy, *Proceedings of the Fourteenth International Conference on Application of Accelerators in Research and Industry*, Denton, 1996, AIP Conf. Proc. No. 392, edited by J. L. Duggan and I. L. Morgan (AIP, Woodbury, NY, 1997).